OPEN BIOLOGY

royalsocietypublishing.org/journal/rsob

Research

Cite this article: Šulskis D, Žiaunys M, Sakalauskas A, Sniečkutė R, Smirnovas V. 2024 Formation of amyloid fibrils by the regulatory 14-3-3ζ protein. *Open Biol.* **14**: 230285. https://doi.org/10.1098/rsob.230285

Received: 17 August 2023
Accepted: 11 December 2023

Subject Area:
biophysics/biochemistry

Keywords:
amyloid, fibrils, 14-3-3ζ, α-synuclein

Author for correspondence:
Darius Šulskis
e-mail: darius.sulskis@gmc.vu.lt

Electronic supplementary material is available online at https://doi.org/10.6084/m9.figshare.c.6991817.

THE ROYAL SOCIETY PUBLISHING

Formation of amyloid fibrils by the regulatory 14-3-3ζ protein

Darius Šulskis, Mantas Žiaunys, Andrius Sakalauskas, Rūta Sniečkutė and Vytautas Smirnovas

Institute of Biotechnology, Life Sciences Center, Vilnius University, Vilnius, Lithuania

DŠ, 0000-0002-6925-4469

The 14-3-3 proteins are a highly conserved adaptor protein family with multi-layer functions, abundantly expressed in the brain. The 14-3-3 proteins modulate phosphorylation, regulate enzymatic activity and can act as chaperones. Most importantly, they play an important role in various neurodegenerative disorders due to their vast interaction partners. Particularly, the 14-3-3ζ isoform is known to co-localize in aggregation tangles in both Alzheimer's and Parkinson's diseases as a result of protein–protein interactions. These abnormal clumps consist of amyloid fibrils, insoluble aggregates, mainly formed by the amyloid-β, tau and α-synuclein proteins. However, the molecular basis of if and how 14-3-3ζ can aggregate into amyloid fibrils is unknown. In this study, we describe the formation of amyloid fibrils by 14-3-3ζ using a comprehensive approach that combines bioinformatic tools, amyloid-specific dye binding, secondary structure analysis and atomic force microscopy. The results presented herein characterize the amyloidogenic properties of 14-3-3ζ and imply that the well-folded protein undergoes aggregation to β-sheet-rich amyloid fibrils.

1. Introduction

14-3-3 are acidic proteins that first were discovered in bovine brain extracts and titled after their migration position in two-dimensional electrophoresis [1]. Afterwards, these proteins were identified as a highly conserved protein family that is found in all eukaryotes [2]. They have been observed to interact with various kinases and enzymes via recognizing phosphorylation sites [3]. Through the vast interaction network, 14-3-3 proteins regulate the activity and stability of proteins, control localization and facilitate protein–protein interactions (PPIs) [4].

There are seven known mammalian isoforms (β, γ, ε, η, ζ, σ and τ/θ) of 14-3-3 proteins [5,6], all of which are dimeric. Each monomer is composed of nine anti-parallel α-helices and a disordered C-terminal tail, which is suggested to have an autoinhibitory role against non-specific interactions [7]. Their overall structure resembles a clamp shape with a conserved amphipathic grove, which is used as an accessible binding site for a plethora of proteins [8]. The different interaction specificity of isoforms comes from individual domain movements that ensure flexible adaptations of the binding surfaces [9].

14-3-3 proteins are found in various human tissues [10], despite being expressed most abundantly in the brain tissues [11]. Most prominently, they regulate important physiological functions such as cell survival, differentiation, migration, apoptosis and ion channel regulation [12]. Due to their involvement in numerous crucial roles in the nervous system, they are also associated with neurodegeneration disorders [13]. Different 14-3-3 isoforms have been found in amyloid plaques (neurofibrillary tangles [14] and Lewy bodies [15]), which are indications of ongoing neurodegenerative diseases [16,17]. Although, they seem to have conflicting roles, as one report demonstrates their ability to facilitate the formation of microtubule-associated tau protein fibrils [18], while another study shows their potential to disrupt tau liquid–liquid phase separation and thus inhibit amyloid aggregation [19]. The increased chaperone-like activity of

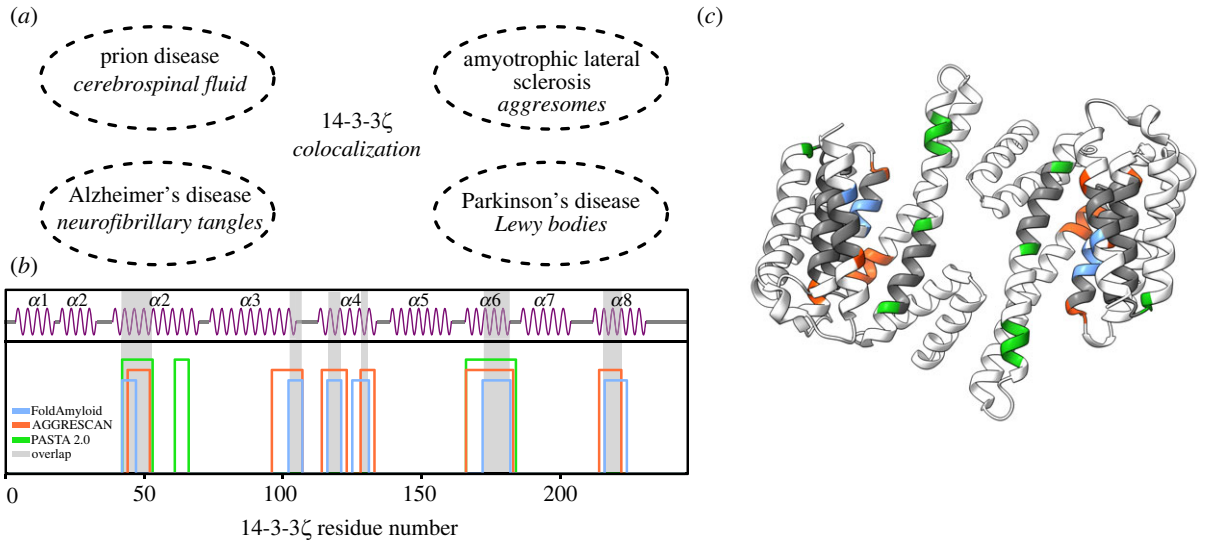

Figure 1. (*a*) 14-3-3ζ co-localization sites in various neurogenerative disorders: in cerebrospinal fluid in prion disease [26,27], in aggresomes during amyotrophic lateral sclerosis [28], in neurofibrillary tangles in Alzheimer's disease [14] and in Lewy bodies during Parkinson's disease [29]. (*b*) Predicted aggregation-prone regions by FoldAmyloid (blue), AGGRESCAN (red) and PASTA 2.0 (green). An overlap with at least two predictors is shown with a grey bar. The secondary structure was depicted using Biotite [30]. (*c*) The predicted aggregation-prone sites are located in α-helices of 14-3-3ζ (PDB Id: 5NAS). The protein structure was visualized with ChimeraX [31].

14-3-3 proteins was observed with Parkinson's disease-related α-synuclein protein [20]. 14-3-3 inhibited α-synuclein aggregation *in vivo* [21] and rerouted its aggregation pathway through binding to intermediate α-synuclein species [22]. Due to these important associations with amyloidogenic and other protein partners, the 14-3-3 family is considered to have a novel therapeutic potential for neurological diseases [16].

While 14-3-3 proteins play a prominent role in neurodegenerative diseases because of their synergy with various partners, it has never been investigated whether they may themselves be susceptible to amyloid aggregation. Previously, there have been several indications that 14-3-3 might be amyloidogenic proteins, since it is known that 14-3-3 share physical and functional homology with α-synuclein [23], particularly in relation to its non-amyloid-β component and C-terminal tail amino acid sequence homology [24]. In addition, it has recently been shown that the concentration of the 14-3-3ζ isoform in cerebrospinal fluid increases during the early stages of Alzheimer's disease [25], indicating a potential link with the disorder pathogenesis.

In this study, we investigated whether the 14-3-3ζ isoform can aggregate into amyloid fibrils. The preliminary computational data showed that the 14-3-3ζ amino acid sequence contains six potential aggregation-prone sites. Subsequently, we monitored protein aggregation using various amyloid-specific dyes and observed gradual, amyloid aggregation over 7 days. The secondary structure analysis confirmed that the exclusively helical protein underwent structural changes and formed β-sheets, akin to the ones found in amyloid fibrils. Finally, atomic force microscopy (AFM) imaging confirmed that 14-3-3ζ aggregates consisted of short, curvy, fibril-like structures.

2. Results and discussion

2.1. 14-3-3ζ contains aggregation-prone regions

14-3-3ζ has been located in various plaques of aggregated proteins in different neurodegenerative diseases. It is possible that strong PPI, leads to their co-localization or even co-aggregation with amyloidogenic proteins (figure 1*a*). As 14-3-3ζ and other family members share similarities to α-synuclein [23,24], which is a main aggregated component of Lewy bodies [20], they can be suspected to be amyloid-forming proteins. Hence, we analysed the 14-3-3ζ amino acid sequence to identify whether 14-3-3ζ contains aggregation-prone regions. We used three different predictors of aggregation-prone sites: FoldAmyloid [32], AGGRESCAN [33] and PASTA 2.0 [34]. The aim was to identify whether 14-3-3ζ has potential aggregation regions and not to quantify them, therefore, each positive site from at least two predictors was characterized as a hit. Overall, results from AGGRESCAN and FoldAmyloid indicated consistent aggregation-prone regions in six sites, whereas PASTA 2.0 only showed three (figure 1*b*). We identified that the six sites, which overlap between different algorithms, are found in five α-helices of 14-3-3ζ (figure 1*b*,*c*). These results matched with previously predicted 14-3-3σ aggregation regions in α2, α3 and α8 helices by PASTA 2.0 and AMYLPRED2 [24], while also suggesting the potential involvement of α4 and α6. Since different predictors indicated that 14-3-3ζ might aggregate, in order to verify that, we examined 14-3-3ζ aggregation properties with various biophysical methods.

2.2. 14-3-3ζ aggregates bind amyloid-specific dyes

For an initial aggregation control assay, the incubated 14-3-3ζ solution was combined with thioflavin-T (ThT) and the sample fluorescence spectra were scanned as described in the Material and methods section. The resulting signal was quite low, which prompted the need for a higher sample concentration prior to the dye assays. The 14-3-3ζ aggregates were pelleted and resuspended into a 10 times lower volume before being used in the assays. Furthermore, in order to account for the possibility of non-amyloid fluorescence enhancement of ThT, three additional dye molecules were used, which included 8-anilinonaphthalene-1-sulfonic acid (ANS) (fluorescence increases in hydrophobic environments) [35], Congo red (CR) (absorbance spectrum

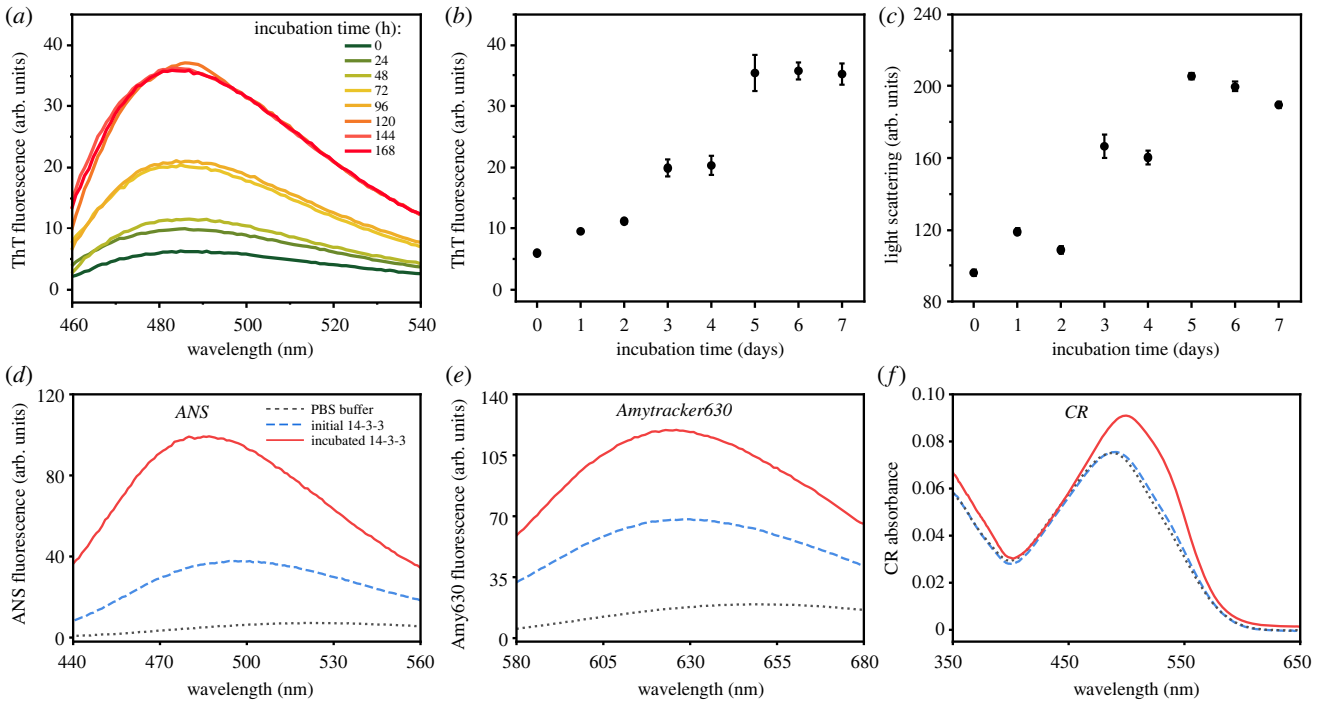

Figure 2. (*a*) The ThT fluorescence spectra of incubated 14-3-3ζ solution at different time points. The ThT fluorescence emission (*b*) and light scattering intensity (*c*) over a 7-day period. The ANS (*e*), Amytracker630 (*e*) fluorescence and CR (*f*) absorbance spectra of PBS buffer, initial 14-3-3ζ at 0 h and incubated for 168 h 14-3-3ζ solutions.

changes upon binding to amyloid fibrils) [36] and a commercial dye, Amytracker 630, which recently has been shown to have very strong photophysical properties when binding to amyloid fibrils [37].

When comparing the intensity of ThT in PBS or with the initial (0 h) 14-3-3ζ solution, there were virtually no differences between the spectra (figure 2*a*). Over the 7 days of incubation, we measured the 14-3-3ζ solution and observed a significant increase in the fluorescence emission intensity with a maximum at 485 nm (figure 2*a*,*b*). The increase in sample light scattering also confirmed the formation of larger structures (figure 2*c*). In the case of ANS, the aggregated 14-3-3ζ solution had the highest signal value (figure 2*d*); however, the 14-3-3ζ solution at 0 h also displayed a considerable level of fluorescence. Similar results were obtained when using Amytracker630 (figure 2*e*), suggesting that 14-3-3ζ was capable of incorporating these molecules, with most likely them binding in the hydrophobic patch within the binding groove [4]. When CR was combined with the aforementioned solutions, only the incubated 14-3-3ζ sample displayed a significant change in the absorbance spectra (figure 2*f*), with the appearance of a shoulder at 540 nm. Such a shift is usually associated with the interaction between CR and amyloid fibrils, as is the increase in total absorbance in the 450–600 nm range [36]. In general, we used four different fluorescence dyes to confirm the amyloid nature of 14-3-3ζ aggregates. Both ThT and CR bind cross-β sheet structures in amyloid fibrils [36,38], which indicates that there are structural transitions in the 14-3-3ζ protein during aggregation, which could change 14-3-3ζ function or interactions with other proteins.

2.3. Formation of β-sheets in 14-3-3ζ aggregates

In the case of monomeric 14-3-3ζ, the Fourier-transform infrared spectroscopy (FTIR) spectrum main maximum position was at 1651 cm^{-1} (associated with the presence of α-helical secondary structure [39]) (figure 3*a*). When 14-3-3ζ was in its aggregated state, the FTIR spectrum main maximum position shifted towards 1638 cm^{-1} and we observed the appearance of an additional minor band at 1695 cm^{-1} (possibly anti-parallel β-sheets). The second derivative of the monomeric 14-3-3ζ FTIR spectrum had a main minimum at 1654 cm^{-1}. Oppositely, the main minimum of the aggregated 14-3-3ζ FTIR spectrum second derivative was at 1631 cm^{-1} (associated with β-sheets) and two other clear minima at 1657 cm^{-1} (α-helices or turns) and 1695 cm^{-1} (anti-parallel β-sheets) (figure 3*b*).

As complementary to FTIR data, we recorded CD spectra of 14-3-3ζ monomers and aggregates (figure 3*c*). The monomer spectrum had two minimum peaks at 209 nm and 223 nm, which is typical for α-helical proteins. On the other hand, the incubated sample spectra had only one unusual red-shifted minimum at 226 nm, which previously had been assigned to β-hairpins in other proteins and peptides [40,41]. This also matches with the observed FTIR band at 1695 cm^{-1}, due to the fact that the anti-parallel β-sheet structure is a component of β-hairpins [42].

2.4. 14-3-3ζ aggregates resemble amyloid fibrils

As a final confirmation that 14-3-3ζ assembled amyloid fibrils, we used AFM imaging to observe the structure and shape of formed aggregates. The initial AFM image showed short amyloid fibrils evenly distributed over the surface of the mica (figure 4*a*). Upon closer inspection, we observed straight or slightly curved fibrils (figure 4*b*). The fibril height distribution was spread between 1 nm and 3 nm, with the mean being 1.6 ± 0.4 nm. During the aggregation assay, we were using α-synuclein fibril formation conditions [43], which included rigorous shaking with glass beads that also could induce fragmentation of aggregates. As an

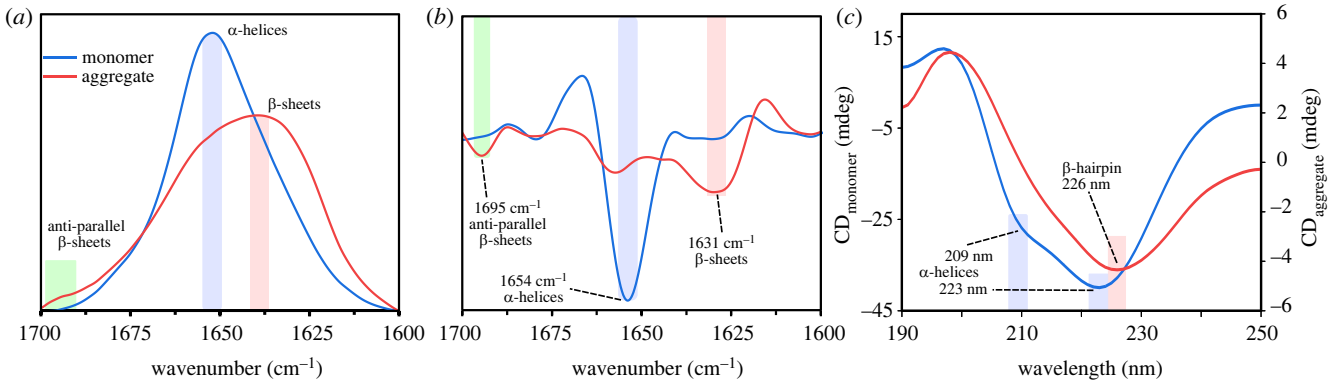

Figure 3. FTIR absorption (*a*), second derivative (*b*) and CD (*c*) spectra of monomeric and aggregate solution of 14-3-3ζ.

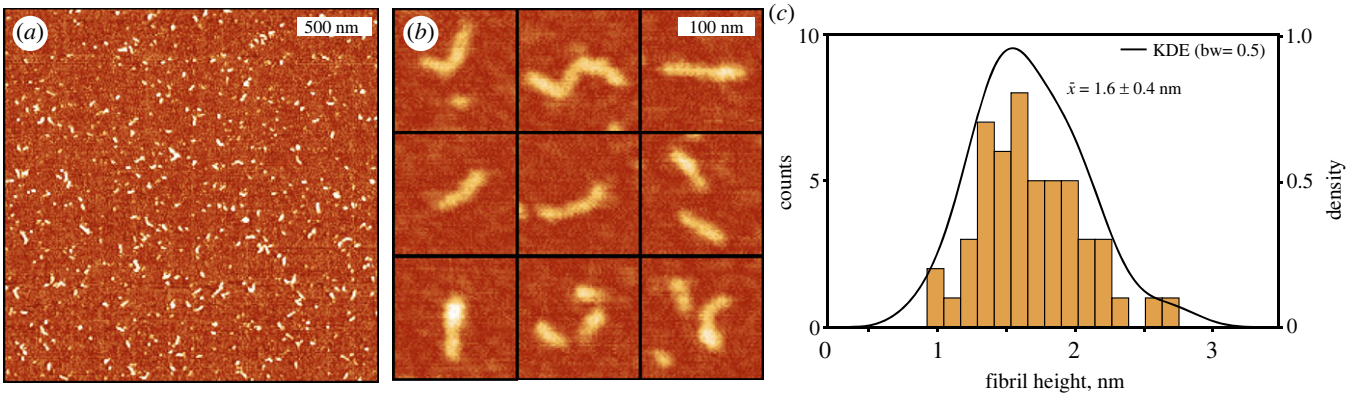

Figure 4. (*a*) AFM image of formed 14-3-3ζ amyloid fibrils (scale bar 500 nm). (*b*) Close-up view of fibrils showing curvy morphology. (*c*) Height distribution of fibrils. The black line is the kernel density estimation (KDE) function fit.

alternative, we tested shaking without glass beads and we observed an increase in ThT fluorescence intensity, but AFM images still only displayed mostly oligomers, with few isolated fibrils (electronic supplementary material, figure S3). Surprisingly, we did find a small number of longer filaments, when it was aggregated at higher protein concentration (200 µM), albeit smaller fibrils still dominated the solution (electronic supplementary material, figure S4). Considering protein concentration might affect protein stability, it may play an important role in determining aggregate length. In all cases, the small shape of the fibrils resembled previously detected worm-like fibrils of the pro-inflammatory S100A9 protein [44] and protofibrils of α-synuclein [45]. These morphological characteristics might be due to large unfolded or still partially folded parts of the protein, which hamper aggregation to long and straight filaments. The FTIR aggregate spectra (figure 3*a*) partially confirmed this, as there was still considerably strong intensity at approximately 1650 cm^{-1}, which corresponds to random-coil or α-helices [39].

2.5. 14-3-3ζ aggregates do not alter α-synuclein aggregation

Since the 14-3-3 protein shares homologous regions with α-synuclein [23], we investigated whether 14-3-3 ζ aggregates can impact α-synuclein aggregation. In the ThT fluorescence assay (figure 5*a*) adding 10% of either 14-3-3ζ native protein or aggregates increased the mean lag time to 10.9 ± 3.4 h and 11.00 ± 0.9 h, respectively, compared to the control 8.5 ± 1.9 h (figure 5*b*); however, a one-way ANOVA showed no significant differences between different groups ($F = 0.47$, $p = 0.63$, $\alpha = 0.05$). Furthermore, the addition of 14-3-3ζ did not change the secondary structure of α-synuclein amyloid fibrils, which indicates that they do not alter the aggregation pathway. AFM imaging also revealed no variations between α-synuclein amyloid fibrils (electronic supplementary material, figure S5). Subsequently, cell toxicity assays of fibrils showed that 14-3-3ζ aggregates reduce cell viability to 65% in the MTT assay (figure 5*d*). The α-synuclein with 14-3-3ζ monomers or aggregates exhibited the same toxicity as the fibrils alone, consistent with our previous observations that α-synuclein fibrils incubated with 14-3-3ζ do not differ from the control.

Overall, we observed that both 14-3-3ζ native protein and aggregates had a limited impact on α-synuclein aggregation. These results could be explained by the fact that 14-3-3 isoforms vary in specificity, as previously it has been confirmed that 14-3-3θ had much stronger chaperone activity for α-synuclein fibril formation [21]. Another consideration is that the 14-3-3 family interacts with phosphorylated targets [46] and in our experimental conditions α-synuclein was not phosphorylated, making it an incompatible target. Nevertheless, the more important part is that 14-3-3ζ aggregates alone can be toxic to the cells and this warrants further experiments to elucidate 14-3-3ζ potential aggregation inside the cell.

3. Conclusion

In this study, for the first time, we observed the formation of amyloid fibrils by 14-3-3ζ. The small shape morphology and relatively weak fluorescence of bound amyloidogenic dyes indicate that 14-3-3ζ fibrils are not easily detectable but

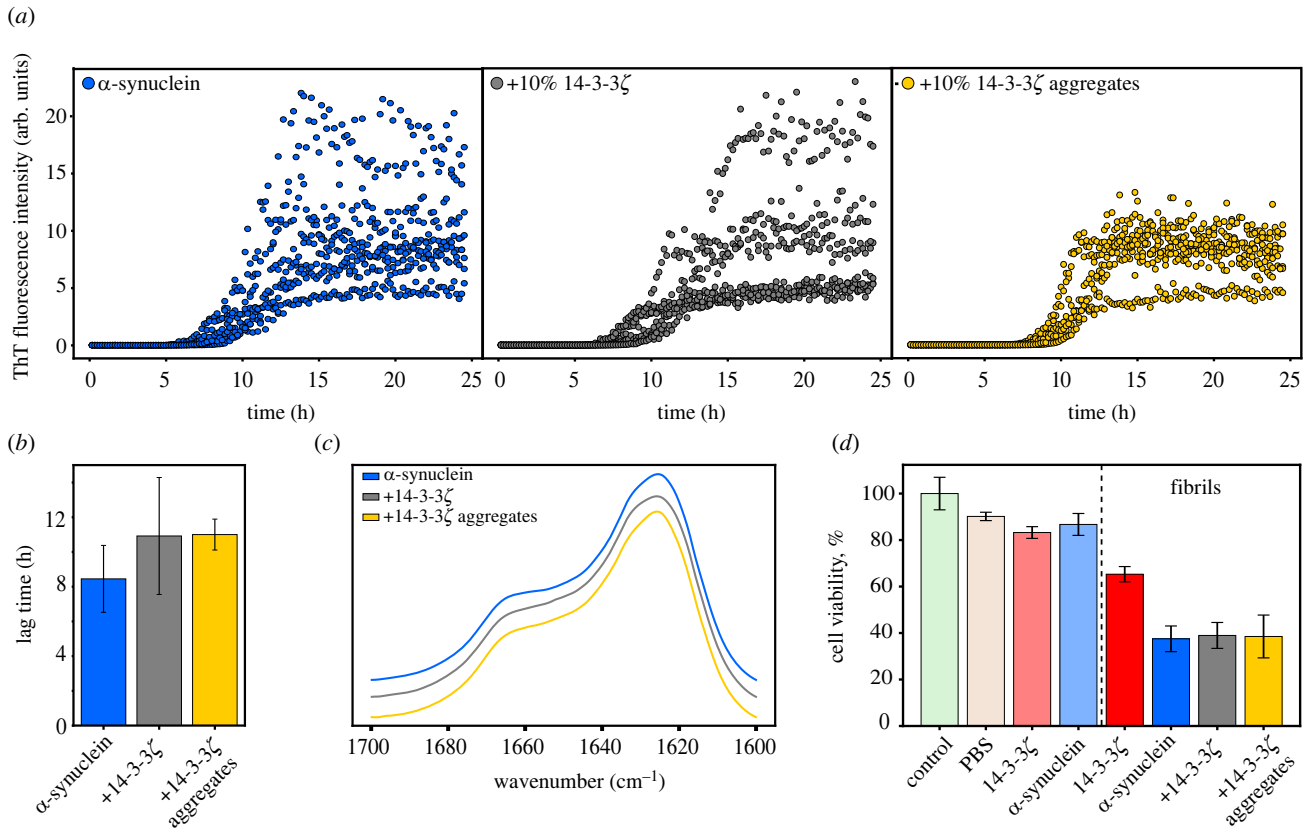

Figure 5. Influence of 14-3-3ζ on α-synuclein aggregation. (*a*) ThT fluorescence kinetics, (*b*) calculated lag times and (*c*) FTIR spectra of α-synuclein fibrils, both alone and co-aggregated with 10% 14-3-3ζ monomers or aggregates. (*d*) Cell viability MTT tests on SH-SY5Y cell in the presence of 14-3-3ζ native protein or aggregates, α-synuclein monomers and α-synuclein fibrils incubated with 10% 14-3-3ζ monomers or aggregates.

exhibit properties that are found in amyloids. Additionally, they were toxic to neuroblastoma cells, but could not accelerate a α-synuclein aggregation, although they share amino acid sequence similarity [24]. Since the detection of 14-3-3 proteins is often associated with the onset of neurodegenerative diseases [25,26,47], our study suggests that this might not only be due to their neuroprotection[48] and chaperone [49] roles but also due to the formation of 14-3-3 fibrils. Moreover, with recent studies indicating 14-3-3 involvement in liquid–liquid phase separation, it is becoming evident that 14-3-3 might have an even larger role in neurodegenerative disorders than initially thought [50,51]. As it is now, the revelation of 14-3-3ζ amyloid properties opens up new possibilities for further investigations into other isoforms of 14-3-3 and their relationship to other protein aggregation pathways.

4. Material and methods

4.1. Protein expression and purification

The 6xHis-SUMO-14-3-3ζ construct used in this work (kind gift of Prof. B.M. Burmann) was derived from GST-14-3-3ζ (Addgene no. 13278) [46]. The plasmid containing 6xHis-SUMO-14-3-3ζ was chemically transformed into One Shot *Escherichia coli* BL21 Star (DE3) (Fisher Scientific) cells. The transformed cells were grown at 37°C in LB medium containing kanamycin (50 mg ml^{-1}) until an optical density at 600 nm ≈ 0.7 was reached. Expression was induced by the addition of 0.4 mM isopropyl-β-D-thiogalactopyranoside (Fisher Scientific), and the cells were left to grow overnight at 25°C. Cells were harvested by centrifugation at 6000*g* for 20 min at 4°C and subsequently resuspended in 50 ml of lysis buffer (25 mM Hepes/NaOH, 1 M NaCl and 10 mM imidazole (pH 7.5)). The suspension was lysed with a Sonopuls (Bandelin) homogenizer (10 s on, 30 s off, 30% power, total time 30 min). Cell debris was removed by centrifugation at 18 000*g* for 45 min at 4°C, and the supernatant was applied to a Ni^{2+} Sepharose 6 Fast Flow (GE Healthcare) loaded gravity column, followed by stepwise elution with 20 ml of lysis buffer supplemented with 100 and 500 mM imidazole, respectively. Fractions containing the 6xHis-SUMO-14-3-3ζ protein were dialysed against phosphate-buffered saline (PBS, pH 7.4), and the 6xHis-SUMO tag was removed by enzymatic cleavage using human sentrin-specific protease 1 (SENP1) catalytic domain (derived from pET28a-HsSENP1) that was a gift from Jorge Eduardo Azevedo (Addgene plasmid no. 71465) at 4°C overnight [52,53]. The primers used for the isolation of the SENP1 catalytic domain gene can be found in electronic supplementary material, table S1. The cleaved proteins were applied again to an Ni^{2+} column, and the flow-through was collected. The proteins were concentrated using Amicon centrifugal filters (10k molecular weight cut-off (MWCO), Merck Millipore) and purified further by size exclusion chromatography (Superdex 75, GE Healthcare) in PBS. The α-synuclein was purified as described previously [54], concentrated to 600 µM and stored at −20°C.

4.2. Aggregation-prone sequence analysis

Predicted 14-3-3ζ aggregation-prone regions were calculated using three different predictors: PASTA 2.0 [34],

FoldAmyloid [32] and AGGRESCAN [33]. The default parameters were used for each prediction. Briefly, in PASTA 2.0 90% sensitivity and −2.8 energy cut-off were used. In FoldAmyloid, aggregation sites were positive, if five successive amino acids with a score above 21.4 were detected. AGGRESCAN identified hot spots of aggregation, whenever the window of five amino acids had an amino acid aggregation-propensity value higher than −0.02. The raw data of predictors results are presented in electronic supplementary material, figure S1.

4.3. 14-3-3ζ and α-synuclein aggregation

The purified 14-3-3ζ or α-synuclein was diluted to 100 µM/200 µM or 100 µM, respectively, using a PBS pH 7.4 solution and distributed to 2.0 ml non-binding test tubes (400 µl volume, each test tube contained two 3 mm glass beads) or Corning non-binding 96-well plates (Fisher, Waltham, MA, USA, cat. no. 10438082) (80 µl volume, each well containing none or one 3 mm glass bead). The samples in tubes were then incubated at 37°C with constant orbital 600 r.p.m. agitation. Every 24 h, three samples were taken for analysis. Samples from 14-3-3ζ 200 µM were taken after 3 and 72 h for AFM imaging. The plates were placed in a ClarioStar Plus plate reader (BMG Labtech, Ortenberg, Germany). The ThT fluorescence measurements were taken every 10 min using 440 nm excitation and 480 nm emission wavelengths every 10 min with constant orbital shaking (600 r.p.m.) in-between at 37°C.

The α-synuclein stock solutions were thawed at room temperature and combined with PBS, 10 mM ThT and monomeric or aggregated 14-3-3 samples (100 µM) to a final α-synuclein concentration of 100 µM, 100 µM ThT and 10 µM 14-3-3. Control solutions contained PBS in place of 14-3-3. Samples were placed in 96-well non-binding plates (100 µl solution, each well contained one 3 mm glass bead). For each condition, six repeats were measured in a ClarioStar Plus plate reader as described before.

4.4. Fluorescence and absorbance assays

For dye-binding assays, ThT, ANS and CR powders were dissolved in PBS buffer solutions and filtered using 0.22 µm syringe filters. The final concentrations of the dye solutions were set to 20 µM (ThT – $\varepsilon_{412} = 23\ 250\ M^{-1}\ cm^{-1}$, ANS – $\varepsilon_{351} = 5\ 900\ M^{-1}\ cm^{-1}$, CR – $\varepsilon_{486} = 33\ 300\ M^{-1}\ cm^{-1}$) based on their specific absorbance spectra, which were scanned using a Shimadzu UV-1800 spectrophotometer. Amytracker630 stock solution was diluted 40 times using PBS buffer prior to use. The prepared dye solutions were stored at 4°C in the dark.

The dye solutions were combined with either PBS, the 14-3-3ζ solution at 0 h or 168 h in a 1 : 1 ratio. The mixtures were then incubated for 10 min in the dark. The fluorescence spectra of ThT, ANS and Amytracker630 were scanned using a Varian Cary Eclipse spectrofluorometer with 10 nm excitation and emission slits, 1 s averaging time and 1 nm intervals (ThT—440 nm excitation and 460–540 emission range, ANS—370 nm excitation and 420–560 emission range, Amytracker630—480 nm excitation and 580–680 nm emission range). The absorbance of CR was scanned from 200 nm to 800 nm using a Shimadzu UV-1800 spectrophotometer. All spectra were corrected using control samples, which did not contain the dye molecules.

4.5. Light scattering assay

Sample right-angle light scattering was scanned with a Varian Cary Eclipse spectrofluorometer, using 600 nm excitation and emission wavelengths with 2.5 nm slit widths, 1 s averaging time.

4.6. Fourier-transform infrared spectroscopy experiments

The aggregated 14-3-3ζ samples (2 ml volume, 100 µM initial protein concentration) and α-synuclein samples (combined six 100 µM repeats of 100 µl initial protein concentration), were centrifuged for 15 min at 12 000*g*. Afterwards, the supernatant was carefully removed and replaced with 500 µl D_2O with 400 mM NaCl (the addition of NaCl improves aggregate sedimentation). The centrifugation and resuspension procedure was repeated three times. After the final centrifugation, the aggregate pellet was resuspended into 50 µl of D_2O with NaCl. The suspension was then scanned as described previously [55] using a Bruker Invenio S FTIR spectrometer. Data analysis was carried out with GRAMS software. D_2O and water vapour spectra were subtracted from the sample spectrum, which was then normalized between 1700 cm^{-1} and 1600 cm^{-1}.

To acquire the FTIR spectra of monomeric 14-3-3ζ, the buffer solution (PBS, pH 7.4) was exchanged into D_2O with 400 mM NaCl using a 10 kDa protein concentrator. The protein solution was diluted to 100 µM using the D_2O solution, placed in the concentrator (400 µl volume) and centrifuged for 10 min at 9000 r.p.m. The concentrated protein solution (approx. 50 µl) was then diluted to the original volume with the addition of 350 µl D_2O. This centrifugation and dilution procedure was repeated four times. The final concentrate was diluted to 100 µl and used for FTIR analysis. The spectra were obtained and analysed the same as the 14-3-3ζ aggregate sample.

4.7. Circular dichroism spectroscopy

All measurements were performed on a Jasco J-815 spectrometer at room temperature. Briefly, either a freshly prepared monomeric solution of 100 µM 14-3-3ζ (PBS, pH 7.4) or aggregated sample was transferred to a 0.1 mm quartz cuvette. Spectra were measured at 1 nm data pitch from 190 nm to 250 nm with a bandwidth of 2 nm and scanning speed of 50 nm min^{-1}. The final spectra of each sample were averaged from three scans with the buffer background subtracted. Analysis and visualization of spectra were done in Spectragryph software (http://spectragryph.com).

4.8. Atomic force microscopy measurements

AFM imaging was done similarly to that previously described [56]. In brief, a 40 µl sample of aggregated 14-3-3ζ was placed on freshly cleaved mica that was functionalized using 40 µl of APTES ((3-Aminopropyl) triethoxysilane), incubated for 5 min. Then the mica was washed with 2 ml MiliQ water and dried gently under a stream of air. High-resolution

images (1024 × 1024) were collected using Dimension Icon (Bruker) AFM operating in tapping mode (Tap300AI-G silicon cantilever (40 N^{-1} m^{-1}, Budget Sensors)). AFM image flattening and fibril analysis were done using Gwyddion v2.57 [57]. The additional AFM images of 14-3-3ζ aggregates can be found in electronic supplementary material, figure S2.

4.9. Cell culturing

SH-SY5Y human neuroblastoma cells were obtained from the American Type Culture Collection (ATCC, Manassas, VA, USA). The cells were grown in Dulbecco's modified Eagle's medium (DMEM) (Gibco, Grand Island, NY, USA), supplemented with 10% fetal bovine serum (FBS) (Sigma-Aldrich, St Louis, MO, USA), 1% penicillin–streptomycin (10 000 U ml^{-1}) (Gibco) at 37°C in a humidified, 5% CO_2 atmosphere in a CO_2 incubator.

4.10. Cytotoxicity of 14-3-3 fibrils

For the MTT assay, SH-SY5Y cells were seeded in a 96-well plate (approx. 15 000 cells $well^{-1}$) and cultured overnight. The 14-3-3ζ, α-synuclein monomers or fibrils in PBS were diluted to a final concentration of 5 µM with DMEM and used to replace the cell medium in each well. After 48 h of incubation, 10 µM of MTT was added to each well and left to incubate for 2 h. One hundred microlitres of 10% SDS with 0.01 M HCl solution was added on top to dissolve formazan crystals. Absorbances at 540 nm, 570 nm and 690 nm (reference wavelength) of each well were measured using a ClarioStar Plus plate reader (BMG Labtech).

Ethics. This work did not require ethical approval from a human subject or animal welfare committee.

Data accessibility. The kinetic and FTIR, CD data used for analysis have been tabulated and are available on Mendeley Data: 10.17632/564277pjyx.1. All other relevant data are available from the corresponding author upon reasonable request.

Supplementary material is available online [58].

Declaration of AI use. We have not used AI-assisted technologies in creating this article.

Authors' contributions. D.Š.: conceptualization, formal analysis, investigation, methodology, visualization, writing—original draft, writing—review and editing; M.Ž.: formal analysis, investigation, methodology, writing—review and editing; A.S.: formal analysis, investigation, methodology, writing—review and editing; R.S.: formal analysis, investigation, methodology; V.S.: supervision, writing—review and editing.

All authors gave final approval for publication and agreed to be held accountable for the work performed therein.

Conflict of interest declaration. The authors declare that they have no competing interests.

Funding. This research received no specific grant from any funding agency in the public, commercial or not-for-profit sectors.

Acknowledgements. The authors thank Björn Marcus Burmann and Jorge Eduardo Azevedo for gifting 6xHis-SUMO-14-3-3ζ and pET28a-HsSENP1 (Addgene plasmid no. 71465) plasmids accordingly.

References

1. Palladin AV, Smerchinskaia LS. 1967 Acidic proteins specific for the nervous system. *Ukr. Biokhimicheskii Zh.* **43**, 398–405.
2. Aitken A, Collinge DB, van Heusden BPH, Isobe T, Roseboom PH, Rosenfeld G, Soll J. 1992 14-3-3 proteins: a highly conserved, widespread family of eukaryotic proteins. *Trends Biochem. Sci.* **17**, 498–501. (doi:10.1016/0968-0004(92)90339-B)
3. Gogl G, Tugaeva KV, Eberling P, Kostmann C, Trave G, Sluchanko NN. 2021 Hierarchized phosphotarget binding by the seven human 14-3-3 isoforms. *Nat. Commun.* **12**, 2–13. (doi:10.1038/s41467-021-21908-8)
4. Obsil T, Obsilova V. 2011 Structural basis of 14-3-3 protein functions. *Semin. Cell Dev. Biol.* **22**, 663–672. (doi:10.1016/j.semcdb.2011.09.001)
5. Martin H, Patel Y, Jones D, Howell S, Robinson K, Aitken A. 1993 Antibodies against the major brain isoforms of 14-3-3 protein: an antibody specific for the N-acetylated amino-terminus of a protein. *FEBS Lett.* **331**, 296–303. (doi:10.1016/0014-5793(93)80356-Y)
6. Ichimura T, Isobe T, Okuyama T, Takahashi N, Araki K, Kuwano R, Takahashi Y. 1988 Molecular cloning of cDNA coding for brain-specific 14-3-3 protein, a protein kinase-dependent activator of tyrosine and tryptophan hydroxylases. *Proc. Natl Acad. Sci. USA* **85**, 7084–7088. (doi:10.1073/pnas.85.19.7084)
7. Truong AB, Masters SC, Yang H, Fu H. 2002 Role of the 14-3-3 C-terminal loop in ligand interaction. *Proteins* **49**, 321–325. (doi:10.1002/prot.10210)
8. Liu D, Bienkowska J, Petosa C, Collier RJ, Fu H, Liddington R. 1995 Crystal structure of the zeta isoform of the 14-3-3 protein. *Nature* **376**, 191–194. (doi:10.1038/376191a0)
9. Yang X, Lee WH, Sobott F, Papagrigoriou E, Robinson CV, Grossmann JG, Sundström M, Doyle DA, Elkins JM. 2006 Structural basis for protein–protein interactions in the 14-3-3 protein family. *Proc. Natl Acad. Sci. USA* **103**, 17 237–17 242. (doi:10.1073/pnas.0605779103)
10. Wang M, Herrmann CJ, Simonovic M, Szklarczyk D, Mering C. 2015 Version 4.0 of PaxDb: protein abundance data, integrated across model organisms, tissues, and cell-lines. *Proteomics* **15**, 3163–3168. (doi:10.1002/pmic.201400441)
11. Boston PF, Jackson P, Thompson RJ. 1982 Human 14-3-3 protein: radioimmunoassay, tissue distribution, and cerebrospinal fluid levels in patients with neurological disorders. *J. Neurochem.* **38**, 1475–1482. (doi:10.1111/j.1471-4159.1982.tb07928.x)
12. Berg D, Holzmann C, Riess O. 2003 14-3-3 proteins in the nervous system. *Nat. Rev. Neurosci.* **4**, 752–762. (doi:10.1038/nrn1197)
13. Steinacker P, Aitken A, Otto M. 2011 14-3-3 proteins in neurodegeneration. *Semin. Cell Dev. Biol.* **22**, 696–704. (doi:10.1016/j.semcdb.2011.08.005)
14. Umahara T, Uchihara T, Tsuchiya K, Nakamura A, Iwamoto T, Ikeda K, Takasaki M. 2004 14-3-3 proteins and zeta isoform containing neurofibrillary tangles in patients with Alzheimer's disease. *Acta Neuropathol.* **108**, 279–286. (doi:10.1007/s00401-004-0885-4)
15. Kawamoto Y, Akiguchi I, Nakamura S, Honjyo Y, Shibasaki H, Budka H. 2002 14-3-3 proteins in Lewy bodies in Parkinson disease and diffuse Lewy body disease brains. *J. Neuropathol. Exp. Neurol.* **61**, 245–253. (doi:10.1093/jnen/61.3.245)
16. Pair FS, Yacoubian TA. 2021 14-3-3 proteins: novel pharmacological targets in neurodegenerative diseases. *Trends Pharmacol. Sci.* **42**, 226–238. (doi:10.1016/j.tips.2021.01.001)
17. Irvine GB, El-Agnaf OM, Shankar GM, Walsh DM. 2008 Protein aggregation in the brain: the molecular basis for Alzheimer's and Parkinson's diseases. *Mol. Med.* **14**, 451–464. (doi:10.2119/2007-00100.Irvine)
18. Hernández F, Cuadros R, Avila J. 2004 Zeta 14-3-3 protein favours the formation of human tau fibrillar polymers. *Neurosci. Lett.* **357**, 143–146. (doi:10.1016/j.neulet.2003.12.049)
19. Liu Y-Q, Liang C-Q, Chen Z-W, Hu J, Hu J-J, Luo Y-Y, Chen Y-X, Li Y-M. 2023 14-3-3ζ participates in the phase separation of phosphorylated and glycated tau and modulates the physiological and pathological functions of tau. *ACS Chem. Neurosci.* **14**, 1220–1225. (doi:10.1021/acschemneuro.3c00034)
20. Spillantini MG, Schmidt ML, Lee VM, Trojanowski JQ, Jakes R, Goedert M. 1997 Alpha-synuclein in Lewy bodies. *Nature* **388**, 839–840. (doi:10.1038/42166)
21. Underwood R, Gannon M, Pathak A, Kapa N, Chandra S, Klop A, Yacoubian TA. 2021 14-3-3 mitigates alpha-synuclein aggregation and toxicity in the *in vivo* preformed fibril model. *Acta*

Neuropathol. Commun. **9**, 13. (doi:10.1186/s40478-020-01110-5)

22. Plotegher N *et al.* 2014 The chaperone-like protein 14-3-3η interacts with human α-synuclein aggregation intermediates rerouting the amyloidogenic pathway and reducing α-synuclein cellular toxicity. *Hum. Mol. Genet.* **23**, 5615–5629. (doi:10.1093/hmg/ddu275)
23. Ostrerova N, Petrucelli L, Farrer M, Mehta N, Choi P, Hardy J, Wolozin B. 1999 α-Synuclein shares physical and functional homology with 14-3-3 proteins. *J. Neurosci.* **19**, 5782–5791. (doi:10.1523/jneurosci.19-14-05782.1999)
24. Evans SR, West C, Klein-Seetharaman J. 2021 Similarity of the non-amyloid-β component and C-terminal tail of monomeric and tetrameric alpha-synuclein with 14-3-3 sigma. *Comput. Struct. Biotechnol. J.* **19**, 5348–5359. (doi:10.1016/j.csbj.2021.09.011)
25. Lu Y. 2022 Early increase of cerebrospinal fluid 14-3-3ζ protein in the Alzheimer's disease continuum. *Front. Aging Neurosci.* **14**, 941927. (doi:10.3389/fnagi.2022.941927)
26. Satoh JI, Kurohara K, Yukitake M, Kuroda Y. 1999 The 14-3-3 protein detectable in the cerebrospinal fluid of patients with prion-unrelated neurological diseases is expressed constitutively in neurons and glial cells in culture. *Eur. Neurol.* **41**, 216–225. (doi:10.1159/000008054)
27. Baxter HC *et al.* 2002 Specific 14-3-3 isoform detection and immunolocalization in prion diseases. *Biochem. Soc. Trans.* **30**, 387–391. (doi:10.1042/BST0300387)
28. Okamoto Y *et al.* 2011 Colocalization of 14-3-3 proteins with SOD1 in Lewy body-like hyaline inclusions in familial amyotrophic lateral sclerosis cases and the animal model. *PLoS ONE* **6**, 2–7. (doi:10.1371/journal.pone.0020427)
29. Giusto E, Yacoubian TA, Greggio E, Civiero L. 2021 Pathways to Parkinson's disease: a spotlight on 14-3-3 proteins. *npj Parkinson's J.* **7**, 85. (doi:10.1038/s41531-021-00230-6)
30. Kunzmann P, Hamacher K. 2018 Biotite: a unifying open source computational biology framework in Python. *BMC Bioinformatics* **19**, 346. (doi:10.1186/s12859-018-2367-z)
31. Pettersen EF, Goddard TD, Huang CC, Meng EC, Couch GS, Croll TI, Morris JH, Ferrin TE. 2021 UCSF ChimeraX: structure visualization for researchers, educators, and developers. *Protein Sci.* **30**, 70–82. (doi:10.1002/pro.3943)
32. Garbuzynskiy SO, Lobanov M, Galzitskaya OV. 2010 FoldAmyloid: a method of prediction of amyloidogenic regions from protein sequence. *Bioinformatics* **26**, 326–332. (doi:10.1093/bioinformatics/btp691)
33. Conchillo-Solé O, de Groot NS, Avilés FX, Vendrell J, Daura X, Ventura S. 2007 AGGRESCAN: a server for the prediction and evaluation of 'hot spots' of aggregation in polypeptides. *BMC Bioinformatics* **8**, 65. (doi:10.1186/1471-2105-8-65)
34. Walsh I, Seno F, Tosatto SCE, Trovato A. 2014 PASTA 2.0: an improved server for protein aggregation prediction. *Nucleic Acids Res.* **42**, W301–W307. (doi:10.1093/nar/gku399)
35. Bolognesi B *et al.* 2010 ANS binding reveals common features of cytotoxic amyloid species. *ACS Chem. Biol.* **5**, 735–740. (doi:10.1021/cb1001203)
36. Yakupova EI, Bobyleva LG, Vikhlyantsev IM, Bobylev AG. 2019 Congo red and amyloids: history and relationship. *Biosci. Rep.* **39**, BSR20181415. (doi:10.1042/BSR20181415)
37. Morten MJ *et al.* 2022 Quantitative super-resolution imaging of pathological aggregates reveals distinct toxicity profiles in different synucleinopathies. *Proc. Natl Acad. Sci. USA* **119**, e2205591119. (doi:10.1073/pnas.2205591119)
38. Biancalana M, Koide S. 2010 Molecular mechanism of Thioflavin-T binding to amyloid fibrils. *Biochim. Biophys. Acta* **1804**, 1405–1412. (doi:10.1016/j.bbapap.2010.04.001)
39. Barth A. 2007 Infrared spectroscopy of proteins. *Biochim. Biophys. Acta* **1767**, 1073–1101. (doi:10.1016/j.bbabio.2007.06.004)
40. Al-Hilaly YK *et al.* 2017 Alzheimer's disease-like paired helical filament assembly from truncated tau protein is independent of disulfide crosslinking. *J. Mol. Biol.* **429**, 3650–3665. (doi:10.1016/j.jmb.2017.09.007)
41. Gordon DJ, Sciarretta KL, Meredith SC. 2001 Inhibition of β-amyloid(40) fibrillogenesis and disassembly of β-amyloid(40) fibrils by short β-amyloid congeners containing *N*-methyl amino acids at alternate residues. *Biochemistry* **40**, 8237–8245. (doi:10.1021/bi002416v)
42. Muñoz V, Thompson PA, Hofrichter J, Eaton WA. 1997 Folding dynamics and mechanism of β-hairpin formation. *Nature* **390**, 196–199. (doi:10.1038/36626)
43. Ziaunys M, Sakalauskas A, Mikalauskaite K, Smirnovas V. 2021 Polymorphism of alpha-synuclein amyloid fibrils depends on ionic strength and protein concentration. *Int. J. Mol. Sci.* **22**, 12382. (doi:10.3390/ijms222212382)
44. Iashchishyn IA, Sulskis D, Nguyen Ngoc M, Smirnovas V, Morozova-Roche LA. 2017 Finke–Watzky two-step nucleation–autocatalysis model of S100A9 amyloid formation: protein misfolding as 'nucleation' event. *ACS Chem. Neurosci.* **8**, 2152–2158. (doi:10.1021/acschemneuro.7b00251)
45. Lashuel HA, Petre BM, Wall J, Simon M, Nowak RJ, Walz T, Lansbury PT. 2002 α-Synuclein, especially the Parkinson's disease-associated mutants, forms pore-like annular and tubular protofibrils. *J. Mol. Biol.* **322**, 1089–1102. (doi:10.1016/S0022-2836(02)00735-0)
46. Yaffe MB, Rittinger K, Volinia S, Caron PR, Aitken A, Leffers H, Gamblin SJ, Smerdon SJ, Cantley LC. 1997 The structural basis for 14-3-3: phosphopeptide binding specificity. *Cell* **91**, 961–971. (doi:10.1016/S0092-8674(00)80487-0)
47. Nilsson J *et al.* 2022 Cerebrospinal fluid biomarker panel of synaptic dysfunction in Alzheimer's disease and other neurodegenerative disorders. *Alzheimers Dement.* **19**, 1775–1784. (doi:10.1002/alz.12809)
48. Shimada T, Fournier AE, Yamagata K. 2013 Neuroprotective function of 14-3-3 proteins in neurodegeneration. *BioMed Res. Int.* **2013**, 564534. (doi:10.1155/2013/564534)
49. Segal D *et al.* 2023 A central chaperone-like role for 14-3-3 proteins in human cells. *Mol. Cell* **83**, 974–993.e15. (doi:10.1016/j.molcel.2023.02.018)
50. Huang X, Zheng Z, Wu Y, Gao M, Su Z, Huang Y. 2022 14-3-3 proteins are potential regulators of liquid–liquid phase separation. *Cell Biochem. Biophys.* **80**, 277–293. (doi:10.1007/s12013-022-01067-3)
51. Han Y, Ye H, Li P, Zeng Y, Yang J, Gao M, Su Z, Huang Y. 2022 *In vitro* characterization and molecular dynamics simulation reveal mechanism of 14-3-3ζ regulated phase separation of the tau protein. *Int. J. Biol. Macromol.* **208**, 1072–1081. (doi:10.1016/j.ijbiomac.2022.03.215)
52. Panavas T, Sanders C, Butt TR. 2009 SUMO fusion technology for enhanced protein production in prokaryotic and eukaryotic expression systems. In *Methods in molecular biology 497* (eds JM Walker), pp. 303–317. Totowa, NJ: Humana Press.
53. Mendes AV, Grou CP, Azevedo JE, Pinto MP. 2016 Evaluation of the activity and substrate specificity of the human SENP family of SUMO proteases. *Biochim. Biophys. Acta* **1863**, 139–147. (doi:10.1016/j.bbamcr.2015.10.020)
54. Šneideris T, Baranauskiene L, Cannon JG, Rutkiene R, Meškys R, Smirnovas V. 2015 Looking for a generic inhibitor of amyloid-like fibril formation among flavone derivatives. *PeerJ* **2015**, 1–17. (doi:10.7717/peerj.1271)
55. Mikalauskaite K, Ziaunys M, Smirnovas V. 2022 Lysozyme amyloid fibril structural variability dependence on initial protein folding state. *Int. J. Mol. Sci.* **23**, 5421. (doi:10.3390/ijms23105421)
56. Sneideris T, Sakalauskas A, Sternke-Hoffmann R, Peduzzo A, Ziaunys M, Buell AK, Smirnovas V. 2019 The environment is a key factor in determining the anti-amyloid efficacy of EGCG. *Biomolecules* **9**, 1–17. (doi:10.3390/biom9120855)
57. Nečas D, Klapetek P. 2012 Gwyddion: an open-source software for SPM data analysis. *Cent. Eur. J. Phys.* **10**, 181–188. (doi:10.2478/s11534-011-0096-2)
58. Šulskis D, Žiaunys M, Sakalauskas A, Sniečkutė R, Smirnovas V. 2024 Formation of amyloid fibrils by the regulatory 14-3-3ζ protein. Figshare. (doi:10.6084/m9.figshare.c.6991817)